**Atmospheric
Chemistry
and Physics
Discussions**

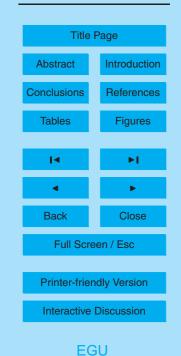**SSA measurement
with X-ray
tomography and gas
adsorption**

M. Kerbrat et al.

Measuring the specific surface area of snow with X-ray tomography and gas adsorption: comparison and implications for surface smoothness

M. Kerbrat[2], B. Pinzer[1], T. Huthwelker[2], H. W. Gäggeler[2,3], M. Ammann[2], and M. Schneebeli[1]

[1]WSL, Swiss Federal Institute for Snow and Avalanche Research SLF, Davos, Switzerland
[2]Paul Scherrer Institute, 5232 Villigen PSI, Switzerland
[3]University of Berne, 3012 Bern, Switzerland

Correspondence to: M. Schneebeli (schneebeli@slf.ch)

Title Page

Abstract	Introduction
Conclusions	References
Tables	Figures

|◄ | ►|

◄ | ►

Back | Close

Full Screen / Esc

Printer-friendly Version

Interactive Discussion

EGU

Abstract

Chemical and physical processes, such as heterogeneous chemical reactions, light scattering, and metamorphism occur in the natural snowpack. To model these processes in the snowpack, the specific surface area (SSA) is a key parameter. In this study, two methods, computed tomography and methane adsorption, which have intrinsically different spatial resolutions –molecular and 30 μm, respectively – were used to determine the SSA of identical natural snow samples. The two methods give identical results, with an uncertainty of 3%. This implies that the surface of natural snow is smooth up to a scale of about 30 μm and that for optical methods a voxel size of 10 μm is sufficient to capture all structural features of natural snow. This smoothness can be physically explained by calculating sublimation and surface diffusion on the snow particles. The methane adsorption method is superior to computed tomography for very fresh snow, but thin layers typical for natural snowpacks can not be resolved. Computed tomography can measure SSA in layers of less than 1 mm thickness, and is therefore advantageous in layered snowpacks.
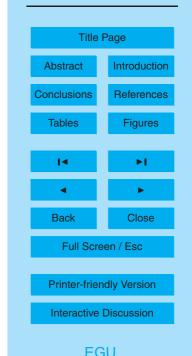
1 Introduction

Snow, after sedimentation of the snow flakes on the surface, has a very high initial porosity and sinters rapidly. Specific surface area is commonly used to describe sintered materials (German, 1996). In the context of integral geometry, specific surface area is identical to the second Minkowski functional (Ohser and Mücklich, 2000). Recently, SSA was found to be a monotonously decreasing parameter apart from volume fraction (Flin et al., 2004; Schneebeli and Sokratov, 2004; Legagneux and Dominé, 2005) in the course of snow metamorphism. This is in contrast to the traditionally used grain size, which has a non-monotonous behavior in the transition from new snow to rounded grain snow to depth hoar (Colbeck et al., 1990). Grenfell and Warren (1999) show that the ratio of volume to surface area (i.e. the inverse of SSA) is the best estima-
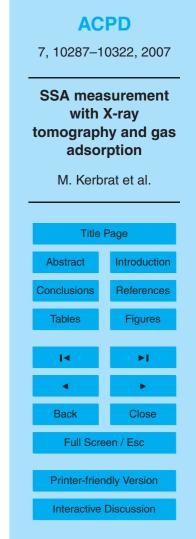
tor for grain size in modelling optics. The same result but with a different optical theory is obtained by Kokhanovsky and Zege (2004). The air permeability of snow can be described using the Carman-Kozeny relation, which uses SSA in developing the hydraulic diameter (Dullien, 1992). Flanner and Zender (2006) use SSA to parameterize snow albedo in the context of global climate models. The interactions between the lower atmosphere and the snowpack is subject to extensive research and it is clear that the chemical reactions which take place in the snowpack depend heavily on the available surface i.e. on the SSA (Grannas et al., 2007). SSA is therefore one of the key parameters in snow physics and chemistry and a precise and unambiguous measurement is necessary.

The SSA of snow has been measured using various techniques, such as determining the adsorption isotherm of nitrogen (Adamson and Dormant, 1966; Adamson et al., 1967; Jellinek and Ibrahim, 1967; Hoff et al., 1998), or of methane at liquid nitrogen temperature (Chaix et al., 1996; Legagneux et al., 2002; Dominé et al., 2007), via the grain size distribution (Granberg, 1985), with stereological measurements (Matzl and Schneebeli, 2007[1]; Narita, 1971; Sommerfeld and Rocchio, 1993), geometrical analysis of images of single snowflakes (Fassnacht et al., 1999), optical and electron microscopy (Dominé et al., 2001), and micro tomography (Flin et al., 2004; Schneebeli and Sokratov, 2004).

Previously published data show considerable scatter, reported values range from 6 up to $77\,700\,\text{cm}^2\text{g}^{-1}$. This is not surprising, because the SSA strongly depends on snow history and snow type. In previous studies, snow history was not specified accurately; it is therefore almost impossible to compare the data obtained with the different techniques. On the other hand, an upper limit of SSA in natural snow covers may be estimated by considering the finest ice structures, which are observed in nature, so called diamond dust (Grenfell and Warren, 1999). These atmospheric long hexagonal

---

[1]Matzl, M. and Schneebeli, M.: Stereological measurement of the specific surface area of snow, J. Microscopy, submitted, preprint at http://www.slf.ch/schnee-lawinen/Schneephysik/Downloads/Stereological_measurement_specific_surf_area.pdf, 2007.

Title Page

Abstract | Introduction

Conclusions | References

Tables | Figures

◀ | ▶

◀ | ▶

Back | Close

Full Screen / Esc

Printer-friendly Version

Interactive Discussion

EGU

ice crystals can have an aspect ratio of 50:1, with a typical diameter as small as 15 μm and a length of 750 μm. Based on this shape, we estimate a geometric SSA of around 3 500 cm^{2}g^{-1}, which can be considered as an upper limit for all natural snow covers and therefore question some of the early measurements which resulted in far too high values. During the last ten years, the reported snow SSA seemed to converge to values between 1600 cm^{2}g^{-1}and 20 cm^{2}g^{-1}, depending on the snow type (e.g. Dominé et al., 2007; Chaix et al., 1996; Legagneux et al., 2002; Flin et al., 2004; Schneebeli and Sokratov, 2004). High SSAs are obtained on fresh snow whereas low SSAs are measured on aged snow. Note that values greater than 1000 cm^{2}g^{-1}are scarce. These measurements show that (i) SSA of snow varies over two orders of magnitude and (ii) a conclusive statement concerning the precision and value of the different methods is not possible without using identical snow samples.
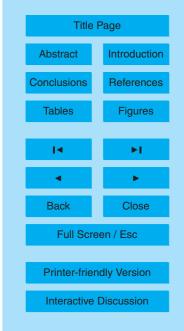
Here, we compared – using identical snow samples – two of the previously cited methods, namely adsorption of methane and X-ray Computed Micro-Tomography (μCT). Methane adsorption measurements followed by BET analysis (Brunauer et al., 1938) have been intensively performed to assess this parameter and a large SSA dataset of natural snow was obtained using this technique (e.g. Dominé et al., 2007; Legagneux et al., 2002). μCT has also been successfully employed in the last decade to investigate geometrical properties of the ice structure and the pore space in snow (Coléou et al., 2001; Flin et al., 2004; Schneebeli and Sokratov, 2004). These techniques have also radically different spatial resolutions. Methane adsorption measurement allows the calculation of accessible surface area from the number of adsorbed molecules and thus has a molecular resolution whereas the used μCT reconstructs the spatial distribution of ice and air with a voxel size of 10 μm, which means that, after filtering, structures of about 30 μm can be clearly resolved. By using two methods having such a different spatial resolution, we also want to address the question of the surface roughness of the ice surface of a snow crystal and the presence of microstructures on its surface. If microstructures exist, the large ratio between the resolutions of the two methods will lead to a disagreement of the measured SSA.

The presence and the size of surface microstructure in high vapour pressure condensed matter, such as ice, is determined by thermodynamic and kinetic processes. Minimization of the Free Energy reduces the overall surface area of the porous medium by sintering. On the contrary, continuous s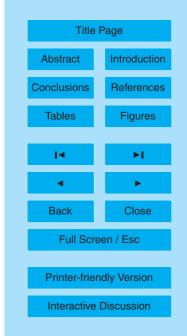ublimation and resublimation of water molecules on the ice surface may induce roughening of the surface and hence the formation of new nanosized structures on the ice surface. The magnitude of such effects depends on the complex interplay of sublimation and resublimation rates, surface and bulk diffusion (Xiao and Ming, 1994). Additional complications occur, because at temperatures above about –20°C, as typical for natural snow, the ice surface is covered by a disordered surface region, which is often called premelt or quasi-liquid layer (see Dash et al., 1995, and citations therein). Because this layer is highly mobile, one might speculate that its thickness defines the scale of the smallest structures on the ice surface. At –5°C, the thickness is of the order of 1 to 10 nm (Henson et al., 2005; Dash et al., 1995; Lied et al., 1994), hence the smallest structures on the ice surface should be larger than this size.

Surface microstructures have been reported on natural snow by Rango et al. (1996) who presented scanning electron microscopy (SEM) images of rimed precipitation particles. Similar microstructures have been seen by Dominé et al. (2003) with the same technique, but they explain these as artefacts due to the resublimation of humid air during the transfer of the samples, which had been stored at liquid nitrogen temperature, into the SEM sample chamber. Nonetheless, even if those observations were artefacts, they show that microstructures can easily form at low temperature. The existence of micro-and nanostructures may affect physical and chemical processes, such as the growth of ice crystals (Libbrecht, 2005, and citations therein), or the total surface area available for trace gas adsorption and chemical reactions on the ice surface.

In this paper, we show that both methods coincide within 3% for SSA ranging from 50 to $700 \, cm^2 g^{-1}$. Therefore the physical concepts, on which the adsorption of methane and μCT are based allow assessing the SSA of natural snow. It also shows that the low spatial resolution of the tomograph compared to an adsorption measurement is

SSA measurement with X-ray tomography and gas adsorption

M. Kerbrat et al.

Title Page

Abstract | Introduction

Conclusions | References

Tables | Figures

◄◄ | ►►

◄ | ►

Back | Close

Full Screen / Esc

Printer-friendly Version

Interactive Discussion

EGU

enough to measure accurately SSA of natural snow. Moreover, it proves that the ice surface of snow is smooth up to a scale of 30 μm.

2 Measurement Procedure

2.1 Sampling

We used five different natural snow types, covering the ranges 2–5 defined in the *International Classification for Seasonal Snow on the Ground* (ICSSG) (Colbeck et al., 1990). These are expected to cover a broad range of SSA. Three types of snow, called "decomposing snow" (*ds*), "metamorphosed I" (*mI*), and "metamorphosed II" (*mII*), were prepared by sieving (in order to avoid creation of inhomogeneities) fresh snow after precipitation into boxes. The boxes were stored at different temperatures, allowing for isothermal metamorphism at different rates. Details of storage are found in Table 1. Two more snow types were collected in the field just before the measurements, denoted "depth hoar" (*dh*), and large grained "wet snow" (*ws*). The *dh* snow was collected in blocks, while the *ws* was also sieved into boxes (10 mm grid) and soaked with ice water to further reduce the SSA. These snow types *ds, mI, mII, dh*, and *ws*, correspond to the ICSSG classes 2a, 3a/2a, 3a, 5a$_2$, and 6a, respectively (see Table 1). The characteristic grain shapes, along with the real 3-D structures, of all five snow types are shown in Fig. 1.
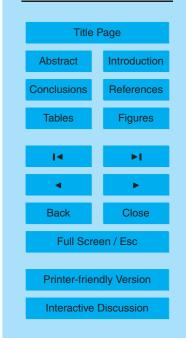
Natural snow covers exhibit density fluctuations and layering on a length scale of various centimeters. Since homogeneity of the snow used for sampling is crucial for comparison of the two methods, we confirmed homogeneity for each block of snow by means of a high resolution penetrometer (Schneebeli et al., 1999). In the region of maximum homogeneity, 7 to 8 cores, each of 57.3 cm^3 volume, were extracted by inserting sharp edged Polyethyleneimine (PEI) sample holders into the snow and carefully removing the remaining snow at the outside of the sample holders. After weighing each cylinder, five were mounted in a specially designed stainless steel sample holder

for the BET measurements, while the remaining samples were directly scanned in the μCT.

2.2 Adsorption of methane

In this study, we used the apparatus already used by Bartels-Rausch et al. (2002, 2004). The adsorption method to determine the SSA of snow using methane has been described by Legagneux et al. (2002). In short, a small amount of gaseous methane is filled into a defined volume. Methane is then expanded into the evacuated sample holder kept at liquid nitrogen temperature, which contains the snow. The pressure drop, due to expansion of the gas into the sample holder and adsorption on the snow surface allows calculating the number of molecules which has adsorbed on the snow surface. This number is calculated using the ideal gas equation. It is assessed from the difference in the gas phase molar budget of methane before and after the expansion. An isotherm of adsorption is obtained by increasing the pressure of methane over snow step by step.

All measurements were made according to a strict protocol as follows. i) The snow sample is thermalized to liquid nitrogen temperature for at least 1 hour. ii) The air is very slowly evacuated from the porous snow sample (≈ 5 mL min^{-1}) using first a primary pump and subsequently a turbo molecular pump. After around 30 minutes, high vacuum ($\approx 10^{-2}$ Pa) is established in the system. The vapour pressure of ice at liquid nitrogen temperature is lower than 1.9×10^{-4} Pa (lowest value from Mauersberger and Krankowsky, 2003, at 164.5 K). Hence, sublimation of ice due to pumping is insignificant. iii) The volume occupied by the snow sample is measured, at least three times, by expanding Helium. Although the u-shaped gas inlet is immersed into liquid nitrogen, the flow of helium was kept at a slow rate of 6×10^{16}-3×10^{17} Molecules s^{-1} to avoid possible annealing of the snow sample due to the introduction of warm gas. iv) The isotherm of adsorption was measured. Sixteen data points were recorded by stepwise increasing the reduced pressure (P/P_0) of methane over snow, where P is the pressure of methane in the system and P_0 is the vapour pressure of methane at liquid nitrogen

temperature. v) Three desorption points were recorded to check the reversibility of the adsorption.

Each isotherm obtained was processed by applying the BET model (Brunauer et al., 1938; Legagneux et al., 2002; Gregg and Sing, 1982). This model describes the adsorption of gases in multimolecular layers. Assuming that an infinite number of layers is formed during the adsorption process, the model leads to Eq. (1),

$$\frac{P/P_0}{N_{ads}\left(1 - P/P_0\right)} = \frac{1}{N_M C} + \frac{C - 1}{N_M C}\frac{P}{P_0}, \tag{1}$$

where N_{ads} is the number of molecules adsorbed per gram of snow, P is the pressure in the system, P_0 is the vapour pressure of methane at liquid nitrogen temperature, N_M is the monolayer capacity (i.e. the total number of molecules that can be adsorbed on a single layer) and C is the so called BET constant.

The measurements were done in Davos, Switzerland, where, due to the altitude, the atmospheric pressure in the laboratory was 828 ($\pm$4) hPa during the experiments. The boiling point temperature of liquid nitrogen at this pressure was derived to be 75.7 ($\pm$0.2) K (Moussa et al., 1966). The vapour pressure of methane at 75.7 K was calculated to be 1030 ($\pm$2) Pa (Lide, 2006).

2.3 Tomography

We used a modified Scanco μCT 80 desktop X-ray computer tomograph, with a microfocus X-ray source emitting a white spectrum (45 kV acceleration voltage), to scan the snow samples. A 180° rotation of the sample was divided into 1000 steps. At each angular step, a 1024×128 CCD detector captured the absorption signal during an integration time of 250 ms, and averaged over two such intervals in order to reduce the noise. The apparatus resides in a cold room at −15°C. With this configuration, a complete scan with 408 slices took approximately 3 h. Along with each adsorption measurement, two or three tomograms were taken, with a voxel size of 10 μm for the

M. Kerbrat et al.

Title Page

Abstract | Introduction

Conclusions | References

Tables | Figures

|◄ | ►|

◄ | ►

Back | Close

Full Screen / Esc

Printer-friendly Version

Interactive Discussion

EGU

fine grained *ds*, *mI*, and *mII* snow types. This corresponds to the maximum resolution of the μCT. For the much coarser *dh* and *ws* types a resolution of 18 μm was chosen, since then a larger volume can be processed. After scanning, a subvolume was extracted from the reconstructed image. After filtering with a 3×3×3 median filter and a 3×3×3 3-D Gaussian kernel filter with a standard deviation of 1.2 voxels a volume of 600×600×400 voxels remains. Hence, the investigated volumes correspond to 144 mm^3 and 839.81 mm^3 for a voxel size of respectively 10 and 18 μm, which can be considered representative for the whole sample. This has been shown by Kaempfer et al. (2005) and Coléou et al. (2001), who found that the elementary volumes, i.e. the minimal volumes which correctly represent the bulk snow properties, are between 1.25^3 and 2.5^3 mm^3, depending on the snow coarseness. The volumes we have used for the analysis are at least ten times larger.

To segment the images we considered the gray scale histograms of the tomograms. Figure 3 shows the histograms of all measurements of two snow types, decomposing snow and depth hoar. One would expect two peaks, representing the two materials ice and air; while this is true for depth hoar, the histogram for decomposing snow is dominated by the air peak. In this case, the fine structure of the *ds* sample leads to many mixed voxels, i.e. voxels with a gray scale value between that of ice and air, and it is difficult to find a threshold value for segmentation. The optimal threshold was determined by fitting a sum of two Gaussian curves to the gray scale histograms and calculating the intersection of the individual Gaussians (Sonka et al., 1999). This procedure minimizes the number of spurious voxels introduced in the segmentation process. The optimal threshold was determined for each tomogram, and the mean for each class was finally applied to segment the images. In Fig. 3, bars indicate the variations around the mean optimal threshold for all measurements of a particular class. This uncertainty in threshold finally leads to an uncertainty in the SSA, where the sensitivity of SSA on threshold variations depends on the snow type and has to be determined experimentally .

3 Results

For each of the *mI*, *mII*, and *dh* types five blocks were investigated, whereas for *ds* and *ws* only four and three blocks, respectively, were used. Thus, 22 adsorption measurements were made, of which 15 were accompanied by three μCT scans, and the remaining seven by two, giving a total of 59 μCT images.
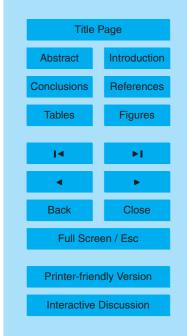
3.1 Adsorption of methane

The mean heat of adsorption (ΔQ_{CH_4}) was derived according to $\Delta Q_{CH_4} = RT \ln C$, using the BET constant C (Legagneux et al., 2002; Gregg and Sing, 1982). For the whole set of measurements we found a mean value of 2680 ($\pm$200) J mol^{-1}. This value is in agreement with the one given by Dominé et al. (2007) who found 2580 ($\pm$200) J mol^{-1}. The adsorption of methane on the sample holder walls may lead to artefacts in the BET analysis, as mentioned by Legagneux et al. (2004). We quantified it by blank measurements and found that the surface area of the wall is 0.278 ($\pm$0.001) m^2. The heat of adsorption on the wall of our Polyethyleneimine/Stainless steel sample holder was measured to be 1760 ($\pm$150) J mol^{-1}. In our case, the contribution of the wall represents 8 to 30% of the total uptake of methane, the more important contribution occurring for coarse snow, which has a low SSA. All the SSA values given here are corrected for the adsorption on the wall of the sample holder.

Measured SSA values range from 48($\pm$1) to 656($\pm$52) cm^{2}g^{-1}. The errors on each value were calculated from both the inherent errors of the experimental apparatus and the errors on physico-chemical data. This specific type of errors was called "a-priori errors". The calculated mean SSA values for each snow type are given in Table 1, where the cited errors are the standard deviations (1σ) of all measurements within each snow type. This error was called "interblock error".

Due to the repetitive injections of methane "a-priori errors" on data points are increasing with rising methane pressure, as Fig. 2 shows. In order to take this into account, each data point was assigned a weight equal to the inverse of its own error. This weight
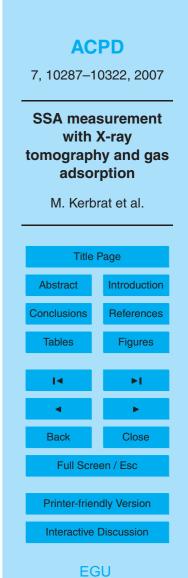
was used when fitting the BET transform of the isotherm (see Fig. 2).

When calculating the "a-priori error" for each data point of the isotherms of adsorption, it was found that it decreases with increasing SSA. This is due to the fact that the more surface is available; the more sensitive is the method. But when SSA values are determined with the BET model, slopes and intercepts have to be determined, and these are assigned with a larger error for higher SSA. However, the second effect is stronger, such that the combined effect results in an increasing overall error when SSA increases.

3.2 Tomography

The SSA values determined by tomography ranged between 46 ($\pm$1) and 733 ($\pm$78) cm^2g^{-1}. In contrast to the BET measurements, where one measurement was taken for one block of snow, several measurements, using different subsamples, have been made for each snow block (see Sect. 2.1). The error on SSA for one individual block is the standard deviation (1σ) of the SSA determined from the different subsamples taken from one single block. This type of error, and the average SSA, were called "intrablock error" and "intrablock SSA", respectively, and are compared to the adsorption results in Fig. 4. The summarized mean SSA values, calculated from the average of all subsamples for each snow type are given in Table 1, where the cited errors are the "interblock errors" (defined in Sect. 3.1). For decomposing snow (*ds* in Fig. 4), there is a wide variation among the different subsamples of each of the 4 blocks (e.g. from 672 to 821 cm^2g^{-1} within one block). Note that in Fig. 4 the mean (intrablock) SSA is shown, and the variation is expressed in the large error bars. Also, within one and the same subsample, the SSA varies between 5% and 10% depending on the position of the investigated subvolume. As Fig. 3 illustrates, the optimal threshold varies notably for the different decomposing snow measurements, and, in addition, the SSA depends heavily on the threshold for this type ($\approx$0.10 cm^2g^{-1} per gray scale unit). Thus, each individual SSA measurement for decomposing snow has an uncertainty of about $\pm$57 cm^2g^{-1} due to the uncertainty in the optimal threshold determination. As this pos-
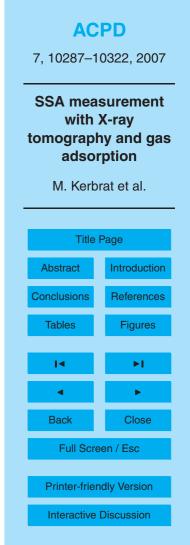
sibly systematic error is smaller than the one estimated from the standard deviation, we chose the standard deviation as error estimate.

On the other hand, the coarse types can be segmented with less ambiguity, thus yielding a sharply determined threshold, and are less sensitive to threshold variation
5 (e.g. for *ws*, $\approx 0.002\,\mathrm{cm^2 g^{-1}}$ per gray scale unit). Therefore, the uncertainty for *ws* measurements, for example, due to thresholding is only $\pm 0.5\,\mathrm{cm^2 g^{-1}}$ for each individual sample. Also, for all other snow types other than decomposing snow, the spatial variation within one scan is less pronounced, i.e. typically about 2%.

3.3   Comparison of data

10 The correlation between SSA values measured by adsorption of methane ($\mathrm{SSA_{BET}}$) and μCT values ($\mathrm{SSA_{\mu CT}}$) was found to be very good. Indeed, the slope of the correlation line, which is shown on Fig. 4, was found to be $\mathrm{SSA_{\mu CT}} = 1.03(\pm 0.03)\mathrm{SSA_{BET}}$. This result was obtained by forcing the linear regression through the origin and assigning a weight to each data point equal to the inverse of the product of the "intrablock errors"
15 on $\mathrm{SSA_{\mu CT}}$ and the "a-priori errors" on $\mathrm{SSA_{BET}}$. This procedure was motivated by the fact that the errors change with the SSA. We note that the correlation is better for lower SSA, which is in agreement with the evolution of the errors on measurements. Moreover, the obtained SSA values are consistent with most recent measurements (Dominé et al., 2007) on comparable snow samples.
20 Albeit the correlation between both methods is very good, the small deviations may be attributed to inherent errors of each method, which are discussed in the two following paragraphs.

Concerning the adsorption measurements, two major sources of error are suspected. i) The molecular area of methane ($a_{\mathrm{CH_4}}$) was experimentally obtained from the molecu-
25 lar area of nitrogen (Chaix et al., 1996). Nonetheless, there is no absolute value of the molecular area of a nitrogen molecule ($a_{\mathrm{N_2}}$), when it is adsorbed on ice. This is mainly due to its dependence on the nature of the surface on which it is adsorbed. Therefore it cannot be defined better than within $\approx$5–10% (Gregg and Sing, 1982). Hence, the

value for the molecular surface area of methane used here ($1.92\times10^{-19}\,\text{m}^2$) also suffers from at least 5–10% uncertainty, which will influence the calculation of SSA. ii) An error of 1 K in the liquid nitrogen temperature determination will give rise to a difference of $\approx$200 Pa in P_0 at a temperature close to the boiling point of liquid nitrogen. From error propagation we estimate an error of about $\approx$3% in the SSA.

Regarding the μCT measurements, the three main sources of error are: i) Setting the threshold value as discussed in Sect. 3.2. ii) Air inclusions in the ice, which could lead to an overestimation of the SSA compared to adsorption, since these pores are not accessible for methane during an adsorption measurement. Analyzing the tomograms, the contribution of such inclusions to the total surface area was found to be always lower than 0.6%, thus being negligible. iii) Choosing a resolution, which is not sufficient to grasp the finest structures of the snow. This would lead to an underestimation of SSA compared to adsorption. Since our values for the finest investigated snow were even slightly above the adsorption values, it may be concluded that structure sizes for this snow type are still of the same order of magnitude as the resolution (10 μm voxel size, corresponding to roughly 30 μm resolution).

To check this hypothesis and to find a limit for the resolution, we gathered and immediately measured solid precipitation, obtaining an adsorption value of 804($\pm$64) and a tomography value of 691($\pm$36) cm^2g^{-1}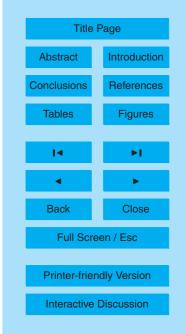. It indicates that precipitation particles still feature structures below about 30 μm, which can be resolved by the gas adsorption method, but not with the resolution of our μCT; we state therefore that for snow the resolution limit of this μCT is approximately 700 cm^2g^{-1}. A theoretical upper limit is given by the SSA of 30 μm cubes, i.e. 2000 cm^2g^{-1}; however, the geometry and distribution of sizes in real structures reduces this theoretical value. Therefore, no theoretical justification for our experimentally found upper limit can be given. Note that this data point, denoted as "Precipitation" in Fig. 4, was not included in the calculation of the correlation coefficient because the μCT value is probably too low due to insufficient resolution.

Apart from the instrumental and analysis issues, also the sampling procedure could

SSA measurement with X-ray tomography and gas adsorption

M. Kerbrat et al.

Title Page

Abstract | Introduction

Conclusions | References

Tables | Figures

◀ | ▶|

◀ | ▶

Back | Close

Full Screen / Esc

Printer-friendly Version

Interactive Discussion

EGU

have induced artefacts. It is well known that a too small sample holder could compress the boundary layer, or break away grains at the boundary. This would lead to an over-estimation or underestimation, respectively, of the weighed density with respect to the density obtained from segmented tomograms. Table 1 shows no significant systematic deviation, however.

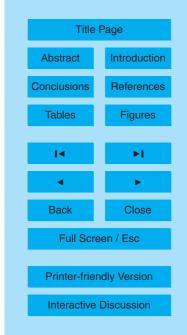## 4 Discussion

4.1 Comparison of methods

Previous studies of the SSA of presumably comparable samples using adsorption method and computer tomography had resulted in the same order of magnitude. For example, Legagneux et al. (2002) measured, using adsorption of methane, the SSA of rounded grains ranging from 400 to 146 cm^2g^{-1} with a mean value for the 15 samples of 249($\pm$80) cm^2g^{-1}. Schneebeli and Sokratov (2004) used the same type of snow for their experiments and measured SSAs of 122 and 218 cm^2g^{-1}.

However, as no direct comparison between both methods has ever been made, it is difficult to assess the quality of methods to determine the SSA of snow. Here, we present the first direct comparison of methods based on two different physical processes and find an agreement within 3% between the SSA values measured by adsorption of methane (SSA_{BET}) and μCT ($SSA_{\mu CT}$), for snow having a SSA below 700 cm^2g^{-1}. This shows that the adsorption of methane and the absorption of X-ray light allow measuring reliably the SSA of snow. It also proves that the data previously obtained using both methods do not suffer from artefacts, such as a lack of resolution or deeper issues, such as problems with physical concepts (e.g. the unknown size of adsorbed methane molecules on the ice surface).

Nonetheless, we showed in Sect. 3.2, that for SSAs higher than around 700 cm^2g^{-1}, tomography underestimates SSA. Taillandier et al. (2007) parameterized the evolution of the SSA of natural snow as a function of temperature for isothermal metamorphism

or under a temperature gradient. If we use this parameterization, we can estimate that for snow having a SSA of 1000 cm^2g^{-1}, it will take 4, 9, 18 or 29 h under temperature gradient conditions at a mean temperature of evolution of the snow layer of –5, –10, –15 and –20°C to cross the limit of quantification of 700 cm^2g^{-1}. In the case of isothermal

5 metamorphism, the times are 7, 12, 19 or 28 h respectively for the same conditions. This shows that the time necessary to reduce the SSA to the limit of detection is short and that the SSA of snow can already be measured successfully with the μCT one day after the precipitation under alpine conditions. Note that we choose 1000 cm^2g^{-1} for the calculation because it is a typical high SSA value and because higher values are

10 rare. Indeed, only 3% of the 340 measurements gathered in Dominé et al. (2007) are greater than 1000 cm^2g^{-1}. To check the validity of the parameterisation on our snow samples, we apply it to our isothermally metamorphosed snow sample. The SSA (SSA$_{Type}$) obtained on our *ds* snow sample was considered as the initial SSA and the times and temperatures given in Table 1 were used in the parameterization.

15 The calculated SSA values are 337 cm^2g^{-1} for *mI* and 260 cm^2g^{-1} for *mII*. Those results agree within 12% and 8% respectively with the one which we measured and show that the parameterization is consistent with our measurements.

4.2 Physical explanation for surface smoothing

Our measurements not only show the coincidence between both methods, but also
20 prove experimentally that our snow samples were smooth up to about 30 μm.

Two mechanisms may be capable of smoothing the ice surface and therefore would explain our experimental results: vapour transport due to the Kelvin effect (Flin et al., 2003; Legagneux and Dominé, 2005), and surface diffusion. The latter process might be quite fast on the ice surface due to the presence of a highly mobile surface layer,
25 often called premelt layer or quasi liquid layer (e.g. Dash et al., 1995).

To see whether our observations are consistent with these principles, here we give a simple estimation of the time scale a small spherical asperity would need to completely disappear from a flat surface.

According to the Kelvin effect, the vapour pressure above a convex interface is enhanced compared to the one above a flat surface (Pruppacher and Klett, 1997). First, for the Kelvin effect, we consider a simple configuration like a half sphere emerging from a flat surface. The higher water vapour pressure above the curved surface as compared to the flat surface results in sublimation of the curved asperity, where the water vapour is transported away by gas phase diffusion. Even for such a simple configuration, the kinetics of how the half sphere will sublimate would require a numerical simulation. As such a calculation is far beyond the scope of this paper; we simplify the geometry and neglect the flat surface where the half sphere rests. Considering only a flat surface at infinite distance from the half sphere, an analytic solution for this diffusion problem can be obtained. The effect of a flat surface beneath the half sphere is an increase of the pressure gradient, implying an increase of the diffusion flux. In this sense our estimation yields an upper limit for the diffusion time. Three different conceptual models were tested to see if the evaporation time depends on the way how the asperity evaporates. The three ways of evolution are illustrated in Fig. 5. The characteristics of each model are: i) The radius of the asperity – and therefore the water vapour flux from the evaporating asperity under steady state conditions – is assumed to be constant until the asperity has disappeared when the amount of water it contained has been diffused away, ii) the radius of the asperity decreases during sublimation, which leads to an increase of the water flux as the radius gets smaller. When the radius reaches 0, the asperity has disappeared, iii) the contact area of the asperity with the flat surface is kept constant and the asperity will flatten, hence the water vapour flux will decrease. The asperity is considered flat when the radius of curvature has grown to 1000 times the original radius of curvature. (details see Appendix A). The results of the calculations are shown in Fig. 6. The different models coincide within at most 6% for the radii under consideration and the difference due to the different assumptions cannot be seen in Fig. 6.

Second, the effect of surface diffusion on the smoothing of asperities may be estimated by calculating the order of magnitude of the time it takes to smear out the

asperity by the random movement of molecules on the highly mobile surface. The surface diffusion constant D_s has been determined in the past in a number of different experiments, but the results depend heavily on the method and on the temperature range of the measurement (Mizuno and Hanafusa, 1987; Brown and George, 1996; Livingston et al., 1997; Jung et al., 2004). Here, we quote the work of Mizuno and Hanafusa (1987), since they measured the properties in the quasi liquid layer on a collection of small ice beads at temperatures close to the melting point, which resembles the situation in snow. Using NMR spectroscopy between −1.5 and −20˚C, they found an activation energy of $E_a = 0.24$ eV and a preexponential factor of $D_0 = 8.43 \times 10^{-9}$ m^{2}s^{-1}.

Using these assumptions, and the characteristic diffusion length of $\Delta x = (4D_s\, t_d)^{1/2}$, we can estimate the characteristic time t_d to distribute an asperity of radius R into a disc of thickness d

$$t_d = \frac{R^3}{6 d D_s}. \tag{2}$$

To estimate an upper limit for the timescale, we consider that the asperity is completely smeared out when it has reached the thickness of the quasi-liquid layer. However, measurements of the thickness of the quasi-liquid layer are subject to discrepancies. The fact that the techniques used to measure it are sensitive to different physical features of the quasi-liquid layer properties could explain the differences (Huthwelker et al., 2006). Several theoretical models related to the quasi-liquid layer have also been developed (Dash et al., 1995), but the experimental discrepancies render it difficult to decide which model is the most appropriate. Moreover, it has been shown theoretically that impurities (Wettlaufer, 1999) and curvature (Baker and Dash, 1989) could affect the thickness of the quasi-liquid layer. Hence, the thickness of this layer is not yet exactly established. In this paper our aim is only to evaluate the effect of surface diffusion when flattening an ice surface. Thus, in the calculation, we use an order of magnitude assumption for the quasi-liquid layer thickness, in agreement with published data. Hence, in Fig. 6, the thickness of the quasi-liquid layer was set to 100 and 10

Title Page

Abstract | Introduction

Conclusions | References

Tables | Figures

◀◀ | ▶▶

◀ | ▶

Back | Close

Full Screen / Esc

Printer-friendly Version

Interactive Discussion

EGU

namometer at −1°C and −40°C, respectively. For such thicknesses, the characteristic time for the surface diffusion is 10 times higher, but becomes comparable to vapour diffusion for smaller radii, where the size of the asperity is comparable to the mean free path and diffusion becomes limited by molecular kinetics.

Figure 6 also suggests that even at temperatures as low as −40°C the "smoothing" of the surface due to the Kelvin effect is very fast, and after a day structures of the size of several micrometers have disappeared. This estimate agrees with our measurements. Indeed, if we used Eq. (A6) to calculate the size of the asperities which would still be present on our *ds* sample which was stored 8 days at −50°C, we find that all asperities having a radius lower than 15 μm may have sublimated. This radius corresponds to an asperity of a about 30 μm in size, which is the resolution of the tomograph. As no asperities smaller than the resolution of the tomograph may have "survived" – if they were present after the formation of the crystal –, SSA_{BET} agrees with $SSA_{\mu CT}$ on this decomposing snow sample. In the case of the sample called "Precipitation" (see Sect. 3.3), the latter was measured about one hour after the precipitation. The air temperature during sampling was ≈ -7°C. Using Eq. (A6), we calculated that only asperities with a diameter of about 20 μm and smaller would have had time to sublimate before the measurement. This means that on the "Precipitation" sample there possibly were still asperities which could not be resolved by the tomograph and therefore SSA_{BET} was higher than $SSA_{\mu CT}$. The calculation also shows that during the scan of a sample, which takes 3 h and which is made at −15°C (see Sect. 2.3), all asperities with a diameter of ≈25 μm which may have been present at the beginning of the scan will disappear during the measurement. As this value is lower than the resolution of the tomograph, the changes occurring during the scan will not affect the results. In the case of an adsorption measurement, there is no evolution of the sample during the measurement, as it is done at liquid nitrogen temperature

We saw in the previous paragraphs, that the surface of ice is very likely to be smooth on a micrometer and nanometer scale. Nevertheless, ice is a high vapour pressure (P_0) solid and in thermodynamic equilibrium, its surface is continuously bombarded

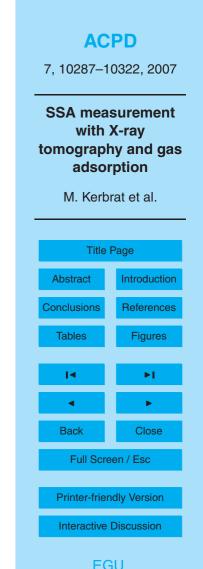**SSA measurement with X-ray tomography and gas adsorption**

M. Kerbrat et al.

with water molecules with a rate of $j_{kin}=P_0\bar{v}/(4k_BT)$ with the mean thermal velocity $\bar{v}=(8k_BT/\pi M)^{1/2}$, while the same flux of water molecules desorbs. In absence of surface diffusion on the ice surface, this continuous exchange of molecules with the gas phase could lead to a molecular rough surface. However, driven by the minimization of the surface energy, the roughness will disappear, if surface diffusion is fast enough. The interplay between absorption, desorption and diffusion is complex and has been subject to molecular dynamics studies. Xiao and Ming (1994) studied this interplay and found conditions for the molecules smoothness of surfaces. Based on their work and using the activation energy of diffusion of E_a=0.24 eV (Mizuno and Hanafusa, 1987), the ice surface should be also smooth on a molecular scale, as long the ice does not grow.

4.3 Practical aspects

Both techniques are suitable to measure reliably the SSA of snow. The measurements require in all cases a relatively constant temperature and A.C. power supply. The application in the field is therefore limited to sites with a good infrastructure. Therefore, it has to be pointed out here that optical methods such as contact spectroscopy (Painter et al., 2007) or near-infrared photography (Matzl and Schneebeli, 2006) are much more appropriate for field work.

4.4 Sampling volume, macroscale resolution and snow stratigraphy

Methane adsorption measures the smallest naturally occurring ice particles. Compared to tomography, this independence of resolution is its largest advantage. However, snowpacks are layered (Colbeck, 1991). In fact, the traditional classification of snow layers underestimates the vertical variation of snow properties substantially (Pielmeier and Schneebeli, 2003) . This is also the case for SSA (Matzl and Schneebeli, 2006). A high vertical spatial resolution is therefore extremely important to understand the exchange processes in a natural snowpack. Methane adsorption works only on a rel-

atively large volume; in our measurements we used a sampling volume of 286.5 cm^3, compared to 0.144 cm^3 for tomography. The use of methane adsorption measurements in simulations of real snowpacks must carefully consider errors introduced by the large sampling volume. This is especially important when photon flux and permeability are
5 calculated.

4.5 Atmospheric implications

Regarding atmospheric chemistry, the water vapour fluxes responsible for the smoothing of the surface after the snow crystal has stopped growing may also influence the partitioning of atmospheric trace gases between the gas and the adsorbed phase within
10 and over the snow pack. Indeed, on the first hand, trace gases which may have been trapped during the crystal growth (Huthwelker, 1999; Kärcher and Basko, 2004), could be released during the surface flattening. Such mechanism would lead to a transport of atmospheric gases from the higher to the lower atmosphere. On the other hand, some could be trapped where ice is growing and therefore would be removed from the
15 gas phase also modifying the atmospheric composition over the snowpack.

5 Conclusions

For the first time ever, we have the performance of two techniques to measure the SSA on snow. Although the two techniques used are based on two different physical concepts, the correlation factor between both methods was found to be 1.03(±0.03),
20 for SSA values ranging between 50 and 700 cm^{2}g^{-1}. The spatial resolution of the adsorption method is on the molecular level, while the effective resolution of the μCT is about 30 μm. Thus, the very good agreement between both measurements excludes the presence of micrometer or nanometer sized surface structures, which would remain undetected with the μCT. Consequently, our measurements prove that the ice surface
25 in alpine snow is smooth up to a scale of about 30 μm few hours after the precipitation.

From simple estimations of the time scales for sublimation (Kelvin effect) and surface redistribution (diffusion in a quasi-liquid layer) of small asperities we draw the conclusion that both processes are capable of smoothing the surface on a length scale of about 30 μm within a few hours.

The absence of surface micro- and nanostructures is significant for the modelling in such diverse fields as friction on snow, snow chemistry, snow optics, and snow metamorphism. In modelling snow metamorphism, for example, a smooth surface allows to ignore all processes which might occur on a scale smaller than a few micrometers.

Another very important implication of these results is that the reliability of the μCT in capturing the geometry of snow is guaranteed. This fact is crucial for further investigations to link physical properties with the geometry of snow, for which the μCT is an ideally suited device.

Appendix A

Diffusion due to Kelvin effect

In this section, we present the equations to estimate the time it takes to evaporate a small spherical particle due to the Kelvin effect, if the transport of vapour is limited by gas phase diffusion. In the following paragraphs, we consider a semi-infinite environment, which means that all quantities refer to a half sphere. We consider a particle sitting on a flat surface, which is assumed not to interact with the gas phase. Under this assumption, and assuming steady state diffusion, the water vapour pressure field over the half sphere may be approximated by the solution of the diffusion equation in spherical symmetry which is:

$$p(r) = p_\infty + \frac{A}{r}. \tag{A1}$$

The Kelvin effect states that over a convex surface the vapour pressure is higher than over a flat surface, which provides the boundary conditions

$$p(R) = p_\infty \exp\left(\frac{C}{R}\right),$$ (A2)

$$C = \frac{2m_{\mathrm{H_2O}}\sigma}{k_\mathrm{B}T\rho_\mathrm{ice}}.$$ (A3)

This determines the constant $A=Rp_\infty\left[\exp\left(\frac{C}{R}\right)-1\right]$. In thermodynamic equilibrium, the diffusion away from the curved surface is given by Fick's law, $j=(D/k_\mathrm{B}T)(A/R^2)$, which, upon multiplication with the surface of a half sphere, gives the particle flux leaving the sphere

$$J(R) = 2\pi\frac{D}{k_\mathrm{B}T}Rp_\infty\left[\exp\left(\frac{C}{R}\right)-1\right].$$ (A4)

Then, the rate of mass loss due to diffusion may be expressed as

$$\frac{\mathrm{d}m}{\mathrm{d}t} = -m_{\mathrm{H_2O}}J(R).$$ (A5)

If we now consider the three models for the evolution of the shape of a spherical asperity assumptions, which were described in Sect. 4 and in Fig. 5, one can evaluate the characteristic time needed to sublimate an asperity from a flat surface.

A1   Assumption 1: constant radius

In the first assumption, we neglect the changing radius during sublimation, i.e. assume a constant diffusion rate. The time it takes for a half sphere to evaporate can be calcu-

lated from the analytical solution of equation (A5) as

$$t = \frac{\gamma}{3} \frac{R^2}{\left[\exp\left(\frac{C}{R}\right) - 1\right]},$$ (A6)

$$\gamma = \frac{\rho_{ice} k_B T}{m_{H_2O} D p_\infty}.$$ (A7)

In this assumption, the asperity has disappeared when its total mass has been diffused.

A2   Assumption 2: shrinking sphere

Alternatively we can assume that the radius decreases while the sphere evaporates. The asperity will be considered to have vanished when its radius is zero. In Eq. (A5), the variables can be separated to $dm/dt = dm/dR \cdot dR/dt$. The term dm/dR is the derivative of the mass of a half sphere as function of its radius. The term dR/dt represents the rate of decrease (in this case) of the radius of the particle. The time it takes for the radius to decrease from R (the initial radius) to zero is given by

$$t = \gamma \int_0^R \frac{R'}{\left[\exp\left(\frac{C}{R'}\right) - 1\right]} dR',$$ (A8)

with γ and C as before.

A3   Assumption 3: constant contact area

5   A third model can be constructed by assuming that the contact area between the asperity and the flat surface stays constant, and the radius of curvature increases. The asperity is considered to be flat when its radius has grown to 1000 times the initial radius.

EGU

With the height of a spherical calotte $h = R - \sqrt{R^2 - R_i^2}$ and its volume $V = \frac{\pi}{3} h^2 (3R - h)$, we can calculate the derivative

$$\frac{dV}{dR} = \pi R \left(2R - \frac{2R^2 - R_i^2}{\sqrt{R^2 - R_i^2}} \right) . \tag{A9}$$

As $dm/dR = dV/dR \cdot \rho_{\text{ice}}$, Eq. (A5) can be used in the same way as in the assumption 2 and we obtain upon integration:

$$t = \frac{\gamma}{2} \int_R^{R_f} \frac{2R' - \frac{2R'^2 - R_i^2}{\sqrt{R'^2 - R_i^2}}}{\left[\exp\left(\frac{C}{R'}\right) - 1 \right]} \, dR' \tag{A10}$$

The integrals (Eq. A8 and A10) have been solved numerically and the results are shown on Fig. 6. From our calculations, we could state that the way the half sphere evolves upon sublimation doesn't affect the characteristic time it needs to disappear. The diffusion constant has been corrected for kinetic effects for very small spheres, as described in Pruppacher and Klett (1997).

References

Adamson, A. W. and Dormant, L. M.: Adsorption of Nitrogen on Ice at 78 Degrees K, J. Am. Chem. Soc., 88, 2055–2057, 1966. 10289
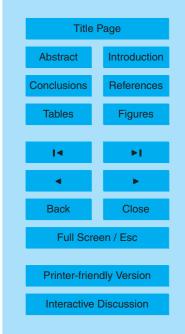
SSA measurement with X-ray tomography and gas adsorption

M. Kerbrat et al.

Title Page

Abstract	Introduction
Conclusions	References
Tables	Figures

ı◀   ▶ı

◀   ▶

Back   Close

Full Screen / Esc

Printer-friendly Version

Interactive Discussion

EGU

Adamson, A. W., Dormant, L. M., and Orem, M.: Physical Adsorption of Vapors on Ice .I. Nitrogen, J. Colloid Interface Sci., 25, 206–217, 1967. 10289

Baker, M. B. and Dash, J. G.: Charge-Transfer in Thunderstorms and the Surface Melting of Ice, J. Cryst. Growth, 97, 770–776, 1989. 10303

Bartels-Rausch, T., Eichler, B., Zimmermann, P., Gäggeler, H. W., and Ammann, M.: The adsorption enthalpy of nitrogen oxides on crystalline ice, Atmos. Chem. Phys., 2, 235–247, 2002,
http://www.atmos-chem-phys.net/2/235/2002/. 10293

Bartels-Rausch, T., Guimbaud, C., Gäggeler, H. W., and Ammann, M.: The partitioning of acetone to different types of ice and snow between 198 and 223 K, Geophys. Res. Lett., 31, L16110, doi:10.1029/2004GL020070, 2004. 10293

Brown, D. E. and George, S. M.: Surface and Bulk Diffusion of $H_2^{18}O$ on Single-Crystal $H_2^{16}O$ Ice Multilayers, J. Phys. Chem., 100, 15 460–15 469, 1996. 10303

Brunauer, S., Emmett, P. H., and Teller, E.: Adsorption of gases in multimolecular layers, J. Am. Chem. Soc., 60, 309–319, 1938. 10290, 10294, 10318

Chaix, L., Ocampo, J., and Domine, F.: Adsorption of CH_4 on laboratory-made crushed ice and on natural snow at 77 K. Atmospheric implications, C. R. Acad. Sci., Ser. II, 322, 609–616, 1996. 10289, 10290, 10298

Colbeck, S., Akitaya, E., Armstrong, R., Gubler, H., Lafeuille, J., Lied, K., McClung, D., and Morris, E.: The International Classification for Seasonal Snow on the Ground, 1990. 10288, 10292

Colbeck, S. C.: The layered character of snow covers, Rev. Geophys., 29, 81–96, 1991. 10305

Coléou, C., Lesaffre, B., Brzoska, J. B., Ludwig, W., and Boller, E.: Three-dimensional snow images by X-ray microtomography, Ann. Glaciol., 32, 75–81, 2001. 10290, 10295

Dash, J. G., Fu, H. Y., and Wettlaufer, J. S.: The Premelting of Ice and Its Environmental Consequences, Rep. Prog. Phys., 58, 115–167, 1995. 10291, 10301, 10303

Dominé, F., Cabanes, A., Taillandier, A. S., and Legagneux, L.: Specific surface area of snow samples determined by CH_4 adsorption at 77 K and estimated by optical, microscopy and scanning electron microscopy, Environ. Sci. Technol., 35, 771–780, 2001. 10289

Dominé, F., Lauzier, T., Cabanes, A., Legagneux, L., Kuhs, W. F., Techmer, K., and Heinrichs, T.: Snow metamorphism as revealed by scanning electron microscopy, Microsc. Res. Tech., 62, 33–48, 2003. 10291

Dominé, F., Taillandier, A. S., and Simpson, W. R.: A parameterization of the specific surface

Title Page

Abstract | Introduction

Conclusions | References

Tables | Figures

|◀ | ▶|

◀ | ▶

Back | Close

Full Screen / Esc

Printer-friendly Version

Interactive Discussion

EGU

area of snow in models of snowpack evolution, based on 340 measurements, J. Geophys. Res., doi:10.1029/2006JF000512, 2007. 10289, 10290, 10296, 10298, 10301

Dullien, F. A. L.: Porous Media: Fluid Transport and Pore Structure, Academic Press Inc., U.S., second edn., 1992. 10289

Fassnacht, S. R., Innes, J., Kouwen, N., and Soulis, E. D.: The specific surface area of fresh dendritic snow crystals, Hydrol. Process., 13, 2945–2962, 1999. 10289

Flanner, M. G. and Zender, C. S.: Linking snowpack microphysics and albedo evolution, J. Geophys. Res., 111, D12208, doi:10.1029/2005JD006834, 2006. 10289

Flin, F., Brzoska, J. B., Lesaffre, B., Cileou, C., and Pieritz, R. A.: Full three-dimensional modelling of curvature-dependent snow metamorphism: first results and comparison with experimental tomographic data, J. Phys. D: Appl. Phys., 36, A49–A54, Sp. Iss., 2003. 10301

Flin, F., Brzoska, J. B., Lesaffre, B., Coleou, C. C., and Pieritz, R. A.: Three-dimensional geometric measurements of snow microstructural evolution under isothermal conditions, Ann. Glaciol., 38, 39–44, 2004. 10288, 10289, 10290

German, R. M.: Sintering Theory and Practice, John Wiley & Sons, Inc., 1996. 10288

Granberg, H.: Distribution of grain sizes and internal surface area and their role in snow chemistry in a sub-Arctic snow cover, Ann. Glaciol., 7, 149–152, 1985. 10289

Grannas, A. M., Jones, A. E., Dibb, J., Ammann, M., Anastasio, C., Beine, H. J., Bergin, M., Bottenheim, J., Boxe, C. S., Carver, G., Chen, G., Crawford, J. H., Dominé, F., Frey, M. M., Guzman, M. I., Heard, D. E., Hemig, D., Hoffmann, M. R., Honrath, R. E., Huey, L. G., Hutterli, M., Jacobi, H. W., Klan, P., Lefer, B., McConnell, J., Plane, J., Sander, R., Savarino, J., Shepson, P. B., Simpson, W. R., Sodeau, J. R., von Glasow, R., Weller, R., Wolff, E. W., and Zhu, T.: An overview of snow photochemistry: evidence , mechanisms and impacts, Atmos. Chem. Phys. Discuss., 7, 4165–4283, 2007, http://www.atmos-chem-phys-discuss.net/7/4165/2007/. 10289

Gregg, S. J. and Sing, K. S. W.: Adsorption, Surface Area and Porosity, Academic Press Limited, London, second edn., 1982. 10294, 10296, 10298

Grenfell, T. C. and Warren, S. G.: Representation of a nonspherical ice particle by a collection of independent spheres for scattering and absorption of radiation, J. Geophys. Res., 104, 31 697–31 709, 1999. 10288, 10289

Henson, B. F., Voss, L. F., Wilson, K. R., and Robinson, J. M.: Thermodynamic model of quasiliquid formation on H_2O ice: Comparison with experiment, J. Chem. Phys., 123, 144707, 2005. 10291

ACPD

7, 10287–10322, 2007

SSA measurement with X-ray tomography and gas adsorption

M. Kerbrat et al.

Title Page

Abstract	Introduction
Conclusions	References
Tables	Figures

|◄ | ►|
◄ | ►

Back | Close

Full Screen / Esc

Printer-friendly Version

Interactive Discussion

EGU

Hoff, J. T., Gregor, D., Mackay, D., Wania, F., and Jia, C. Q.: Measurement of the specific surface area of snow with the nitrogen adsorption technique, Environ. Sci. Technol., 32, 58–62, 1998. 10289

Huthwelker, T.: Experimente und Modellierung der Spurengasaufnahme in Eis, Cuvillier Verlag, Göttingen, 1999. 10306

Huthwelker, T., Ammann, M., and Peter, T.: The uptake of acidic gases on ice, Chem. Rev., 106, 1375–1444, 2006. 10303

Jellinek, H. G. and Ibrahim, S. H.: Sintering of Powdered Ice, J. Colloid Interface Sci., 25, 245–254, 1967. 10289

Jung, K. H., Park, S. C., Kim, J. H., and Kang, H.: Vertical diffusion of water molecules near the surface of ice, J. Chem. Phys., 121, 2758–2764, 2004. 10303

Kaempfer, T. U., Schneebeli, M., and Sokratov, S. A.: A microstructural approach to model heat transfer in snow, Geophys. Res. Lett., 32, L21503, doi:10.1029/2005GL023873, 2005. 10295

Kärcher, B. and Basko, M. M.: Trapping of trace gases in growing ice crystals, J. Geophys. Res., 109, D22204, doi:10.1029/2004JD005254, 2004. 10306

Kokhanovsky, A. A. and Zege, E. P.: Scattering optics of snow, Appl. Opt., 43, 1589–1602, 2004. 10289

Legagneux, L. and Dominé, F.: A mean field model of the decrease of the specific surface area of dry snow during isothermal metamorphism, J. Geophys. Res., 110, F04011, doi:10.1029/2004JF000181, 2005. 10288, 10301

Legagneux, L., Cabanes, A., and Dominé, F.: Measurement of the specific surface area of 176 snow samples using methane adsorption at 77 K, J. Geophys. Res., 107, 4335–4349, 2002. 10289, 10290, 10293, 10294, 10296, 10300, 10318

Legagneux, L., Taillandier, A. S., and Dominé, F.: Grain growth theories and the isothermal evolution of the specific surface area of snow, J. App. Phys., 95, 6175–6184, Part 1, 2004. 10296

Libbrecht, K. G.: The physics of snow crystals, Rep. Prog. Phys., 68, 855–895, 2005. 10291

Lide, D. R.: CRC Handbook of Chemistry and Physics, Taylor and Francis, Boca Raton, FL, 86th edn., 2006. 10294

Lied, A., Dosch, H., and Bilgram, J. H.: Surface Melting of Ice I$_h$ Single-Crystals Revealed by Glancing Angle X-Ray-Scattering, Phys. Rev. Lett., 72, 3554–3557, 1994. 10291

Livingston, F. E., Whipple, G. C., and George, S. M.: Surface and bulk diffusion of HDO on

ultrathin single-crystal ice multilayers on Ru(001), J. Chem. Phys., 108, 2197–2207, 1997. 10303

Matzl, M. and Schneebeli, M.: Measuring specific surface area of snow by near-infrared pho-
tography, J. Glaciol., 52, 558–564, 2006. 10305

5 Mauersberger, K. and Krankowsky, D.: Vapor pressure above ice at temperatures below 170 K,
Geophys. Res. Lett., 30, 1121, doi:10.1029/2002GL016183, 2003. 10293

Mizuno, Y. and Hanafusa, N.: Studies of surface properties of ice using neclear magnetic
resonance, J. Phys., 48, 511–517, 1987. 10303, 10305

Moussa, M. R., Muijlwij.R, and Vandijk, H.: Vapour Pressure of Liquid Nitrogen, Physica, 32,
10   900–912, 1966. 10294

Narita, H.: Specific surface of deposited snow II, Low Temp. Sci., 29, 69–81, 1971. 10289

Ohser, J. and Mücklich, F.: Statistical Analysis of Microstructures in Materials Science, John
Wiley & Sons, Inc., 2000. 10288

Painter, T. H., Molotch, N. P., Cassidy, M., Flanner, M., and Steffen, K.: Contact spectroscopy
15   for determination of stratigraphy of snow optical grain size, J. Glaciol., 53, 121–127, 2007.
10305

Pielmeier, C. and Schneebeli, M.: Stratigraphy and changes in hardness of snow measured
by hand, ramsonde and snow micro penetrometer: a comparison with planar sections, Cold
Reg. Sci. Technol., 34, 393–405, 2003. 10305

20 Pruppacher, H. R. and Klett, J. D.: Microphysics of clouds and precipitation, Kluwer Academic
Publishers, 1997. 10302, 10310

Rango, A., Wergin, W. P., and Erbe, E. F.: Snow crystal imaging using scanning electron
microscopy: I. Precipitated snow, Hydrol. Sci., 41, 219–233, 1996. 10291

Schneebeli, M. and Sokratov, S. A.: Tomography of temperature gradient metamorphism of
25   snow and associated changes in heat conductivity, Hydrol. Process., 18, 3655–3665, Sp.
Iss., 2004. 10288, 10289, 10290, 10300

Schneebeli, M., Pielmeier, C., and Johnson, J. B.: Measuring snow microstructure and hard-
ness using a high resolution penetrometer, Cold Reg. Sci. Technol., 30, 101–114, 1999.
10292

30 Sommerfeld, R. A. and Rocchio, J. E.: Permeability Measurements on New and Equitemper-
ature Snow, Water Resour. Res., 29, 2485–2490, 1993. 10289

Sonka, M., Hlavac, V., and Boyle, R.: Image Processing: Analysis and Machine Vision,
Thomson-Engineering, second edn., 1999. 10295

Title Page

Abstract | Introduction

Conclusions | References

Tables | Figures

◀ | ▶

◀ | ▶

Back | Close

Full Screen / Esc

Printer-friendly Version

Interactive Discussion

EGU

Taillandier, A. S., Dominé, F., Simpson, W. R., Sturm, M., and Douglas, T. A.: The rate of decrease of the specific surface area of dry snow: isothermal versus temperature gradient., J. Geophys. Res., in press, 2007. 10300

Wettlaufer, J. S.: Impurity effects in the premelting of ice, Phys. Rev. Lett., 82, 2516–2519, 1999. 10303

Xiao, R. F. and Ming, N. B.: Surface Roughening and Surface-Diffusion in Kinetic Thin-Film Deposition, Phys. Rev. E, 49, 4720–4723, Part B, 1994. 10291, 10305

SSA measurement with X-ray tomography and gas adsorption

M. Kerbrat et al.

Title Page

Abstract | Introduction

Conclusions | References

Tables | Figures

◄ | ►I

◄ | ►

Back | Close

Full Screen / Esc

Printer-friendly Version

Interactive Discussion

EGU

Table 1. Sample characteristics and preparation methods for the different snow types together with the obtained results. $\rho_{weighed}$ is the snow density calculated after weighing a known volume, whereas ρ_{CT} is the density calculated from the segmented μCT images. Note that the relatively large density error includes both the measurement error and the natural sample variation. The number of adsorption and tomography measurements for each snow type corresponds to Nr. BET and Nr. μCT respectively. The given SSA$_{BET}$ and SSA$_{\mu CT}$ represents the mean values –measured by each method– for each snow type and the errors are "interblock errors " (see Sect. 3). The SSA$_{Type}$ are the mean values of all measurements made on each snow with both methods... The given errors are the corresponding standard deviations (1σ).

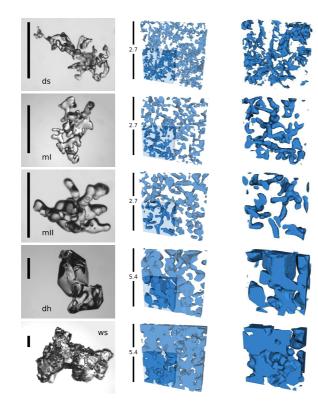| snow type	ICSSG	snow history	$\rho_{weighed}$ g cm^{-3}	ρ_{CT} g cm^{-3}	Nr. BET	Nr. μCT	SSA$_{BET}$ cm^2 g^{-1}	SSA$_{\mu CT}$ cm^2 g^{-1}	SSA$_{Type}$ cm^2 g^{-1}
ds	2a	8 days @ −50°C	0.11 (±0.01)	0.11 (±0.02)	4	11	616(±29)	665(±73)	642(±51)
ml	3a(2a)	14 days @ −17°C	0.15 (±0.01)	0.13 (±0.01)	5	13	346(±11)	420(±27)	381(±42)
mll	3a	17 days @ −3°C	0.19 (±0.05)	0.19 (±0.03)	5	12	270(±31)	291(±27)	282(±30)
dh	5a$_2$	field, not sieved	0.31 (±0.02)	0.31 (± 0.02)	5	14	93(±5)	91(±6)	92(±6)
ws	6a	field, sieved	0.54 (±0.03)	0.56 (± 0.03)	3	9	49(±1)	48(±3)	48(±2)

Fig. 1. Typical grain forms and corresponding 3-D-structures of the different snowtypes: (from top to bottom) decomposing snow, metamorphosed I, metamorphosed II, depth hoar, and wet snow. The scale bar in the left column is always 1 mm. In the middle column, note the different scales of the shown 3-D volumes for fine grained ($2.7{\times}2.7{\times}0.45\,\mathrm{mm}^3$) and coarse grained ($5.4{\times}5.4{\times}0.9\,\mathrm{mm}^3$) snow types. The right column shows a detail of the 3-D structure, i.e. the shaded lower left corner.

Fig. 2. The BET transform (in black on the left axes), is derived from the isotherm of adsorption (in gray on the right axes) (Brunauer et al., 1938). The slope and the intercept of the linear part are used to calculate the SSA (Legagneux et al., 2002).

Fig. 3. Histograms of the filtered 3-D grayscale tomography images. Shown are all tomograms for decomposing snow and depth hoar. The fraction of "mixed voxels" is much higher for decomposing snow (*ds*) than for depth hoar (*dh*). The bars are located at plus and minus one standard deviation of the mean optimal threshold of the individual measurements.

EGU

Fig. 4. The correlation between adsorption measurements and tomography was found to be $SSA_{\mu CT} = 1.03(\pm 0.03)SSA_{BET}$. The plotted error bars given for the adsorption method were called "a-priori errors" whereas the one given for tomography were called "intrablock errors" (see text for details). The data point called "Precipitation" was not taken into account when calculating the correlation coefficient as explained in Sect. 3.3.
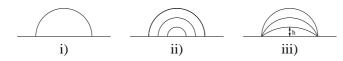
Fig. 5. Models to estimate the sublimation time of a half sphere: i) constant flux ii) decreasing radius, meaning increasing flux, iii) increasing radius
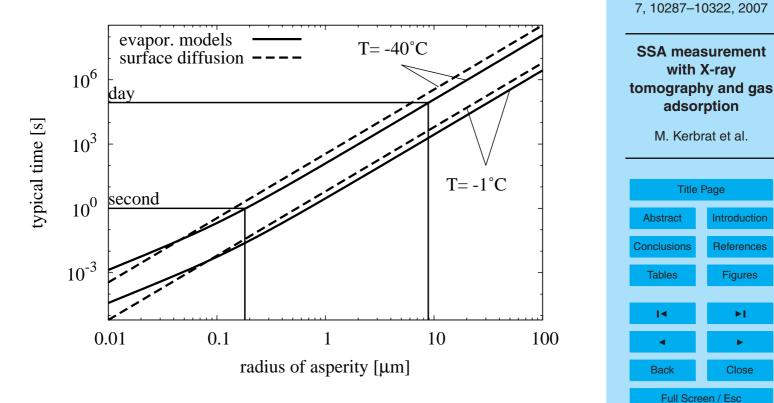
EGU

Fig. 6. Characteristic time for the smoothing of an ice surface due to the Kelvin effect (straight lines) and surface diffusion (dashed lines) as a function of the initial radius of the asperity.

EGU